



UNIVERSITY OF LEEDS

This is a repository copy of *Investigating pitting in X65 carbon steel using potentiostatic polarisation*.

White Rose Research Online URL for this paper:  
<http://eprints.whiterose.ac.uk/117553/>

Version: Accepted Version

---

**Article:**

Mohammed, S [orcid.org/0000-0002-4197-4990](http://orcid.org/0000-0002-4197-4990), Hua, Y, Barker, R [orcid.org/0000-0002-5106-6929](http://orcid.org/0000-0002-5106-6929) et al. (1 more author) (2017) Investigating pitting in X65 carbon steel using potentiostatic polarisation. *Applied Surface Science*, 423. pp. 25-32. ISSN 0169-4332

<https://doi.org/10.1016/j.apsusc.2017.06.015>

---

© 2017 Elsevier B.V. This manuscript version is made available under the CC-BY-NC-ND 4.0 license <http://creativecommons.org/licenses/by-nc-nd/4.0/>

**Reuse**

Items deposited in White Rose Research Online are protected by copyright, with all rights reserved unless indicated otherwise. They may be downloaded and/or printed for private study, or other acts as permitted by national copyright laws. The publisher or other rights holders may allow further reproduction and re-use of the full text version. This is indicated by the licence information on the White Rose Research Online record for the item.

**Takedown**

If you consider content in White Rose Research Online to be in breach of UK law, please notify us by emailing [eprints@whiterose.ac.uk](mailto:eprints@whiterose.ac.uk) including the URL of the record and the reason for the withdrawal request.



[eprints@whiterose.ac.uk](mailto:eprints@whiterose.ac.uk)  
<https://eprints.whiterose.ac.uk/>

# Investigating pitting in X65 carbon steel using potentiostatic polarisation

Sikiru Mohammed <sup>☆</sup>, Yong Hua, R. Barker, A. Neville

*Institute of Functional Surfaces, Department of Mechanical Engineering, University of Leeds, UK*

---

## Abstract

Although pitting corrosion in passive materials is generally well understood, the growth of surface pits in actively-corroding materials has received much less attention to date and remains poorly understood. One of the key challenges which exists is repeatedly and reliably generating surface pits in a practical time-frame in the absence of deformation and/or residual stress so that studies on pit propagation and healing can be performed. Another pertinent issue is how to evaluate pitting while addressing general corrosion in low carbon steel. In this work, potentiostatic polarisation was employed to induce corrosion pits (free from deformation or residual stress) on actively corroding X65 carbon steel. The influence of applied potential (50mV, 100mV and 150mV vs open circuit potential) was investigated over 24h in a CO<sub>2</sub>-saturated, 3.5 wt.% NaCl solution at 30°C and pH 3.8. Scanning electron microscopy (SEM) was utilised to examine pits, while surface profilometry was conducted to measure pit depth as a function of applied potential over the range considered. Analyses of light pitting (up to 120µm) revealed that pit depth increased linearly with increase in applied potential.

This paper relates total pit volume (measured using white light interferometry) to dissipated charge or total mass loss (using the current response for potentiostatic polarisation in conjunction with Faraday's law). By controlling the potential of the surface (anodic) the extent of pitting and general corrosion could be controlled. This allowed pits to be evaluated for their ability to continue to propagate after the potentiostatic technique was employed. Linear growth from a depth of 70µm at pH3.8, 80°C was demonstrated. The technique offers promise for the study of inhibition of pitting.

*Keywords:* X65 carbon steel, CO<sub>2</sub> corrosion, pitting, potentiostatic polarisation and white light profilometry.

---

## 1. Introduction

Low carbon steel such as X65 is widely used as a pipeline material for oil and gas applications [1]. The limitation in carbon steel is in its corrosion resistance, which takes its toll on operations, economy as well as health and safety concerns. Most failures in the oil industry are not due to general corrosion but localised corrosion [2]. Pitting corrosion ranks among the highest level of corrosion defects while pitting in carbon-dioxide (CO<sub>2</sub>) environment remains the most dangerous form of localised corrosion [3, 4]. Pitting is stochastic in nature, hard to predict [3] and can progress without being detected until catastrophe occurs. The danger of localised

corrosion and how to effectively contain it is a growing challenge in the corrosion field [3, 5, 6].

Stochastic pits can be grown by conducting some long term corrosion tests in the laboratory. However, it is desirable to generate pits within a reasonable time-frame for corrosion studies. Some pitting studies have been conducted using artificial pits [7] or by generating pits using mechanical indentation [8, 9] before conducting healing or pit propagation assessments. Other studies such as that by Fang et al. [10] used a needle to remove scales to create pits.

Part of early literature on the artificial pit was that of Newman et al. [11] who studied passivation kinetics in corrosion resistant alloys. Zhuo and Turnbull [12] evolved a two compartment cell arrangement to study stress corrosion cracking in pre-pitted Ni-Cr-Mo-V steel. Turnbull et al.[7, 13] later utilised a similar method to evaluate inhibitors in

---

\*Corresponding author

*Email address:* mnsam@leeds.ac.uk (Sikiru Mohammed <sup>☆</sup>)

their ability to retard localised corrosion. The design entailed separating the anode and cathode compartment but electrically coupled with a zero resistance ammeter (ZRA). Marsh et al. [14] also assessed inhibitor performance in retarding localised corrosion. Their design also utilised a ZRA to measure current between two electrodes of the same material but with different surface area. Han et al. [15] as well developed an artificial pit to investigate localised corrosion of mild steel in CO<sub>2</sub> environment. They investigated galvanic mechanisms involved in the propagation of localised CO<sub>2</sub> corrosion under varying parameters when iron carbonate (FeCO<sub>3</sub>) corrosion products develop on the steel surface. Pit depths of 2mm and flush position were considered. Amri et al. [16] also designed an artificial pit to study the effect of acetic acid on pitting and stifling of carbon steel in CO<sub>2</sub> environment.

While the artificial pit methods described above reveal facts about some pitting properties, their concepts were mainly based on the study of a particular pit profile which does not reflect the random attribute of pitting. It is also difficult to develop artificial pits for pit studies on micro and nano scale levels.

Pitting can also be created using indentation apparatus. Miresmaeili et al. [17] study on X65 steel weld hardness suggested that hardening could halt failure amidst hydrogen presence. Indented pits are however prone to minute cracks arising from deformation/and or residual stress from an indenter's penetration. Such crack tips or local stress state, particularly along grain boundaries could pave the way for hydrogen embrittlement [18, 19, 20].

A potentiostatic approach was utilised by Tian [21] to investigate potential influence on stainless steel pitting in an oxygenated environment based on single pit examination and observed that pit depth increased with time and potential threshold. Tian's potentiostatic experiment was based on a single pit study which does not truly reflect the random properties of pitting in stainless steel. Corrosion in stainless steel could self-heal in certain instances but this is uncertain for low carbon steel which is more prone to corrosion but remains of high demand in oil and gas industry. There is yet no literature that presents a technique to generate reproducible stress free pits of predictable depths on low carbon steel for pit propagation/healing investigations. More so, not much is known about pitting/general corrosion rela-

tionships in low carbon steel.

This work explores the potentiostatic approach supported by robust post-test surface analysis in its ability to generate pitting in X65 carbon steel. Experiments were performed under electrochemical conditions suitable for generating reproducible stress free pits. Since the emergence of pitting does not imply the absence of general corrosion with regard to carbon steel, this work further explores profilometry and potentiostatic application to establish the relationship between general and pitting corrosion in low carbon steel.

## 2. Materials, preparations and experimental procedure

### 2.1. Materials and properties

API X-65 (UNS K03014) grade carbon steel was used for this work. The composition of the steel is given in Table 1 while a micrograph of X65 carbon steel is depicted in Figure 1. The micrograph of

Table 1: Chemical composition (wt%) of X65 carbon steel

C	Si	Mn	P	S	Cr	Mo	Ni
0.12	0.18	1.27	0.008	0.002	0.11	0.17	0.07
Cu	Sn	Al	B	Nb	Ti	V	Fe
0.12	0.008	0.022	0.0005	0.054	0.001	0.057	Balance

low carbon steel features pearlite (dark regions) and ferrite (bright regions).

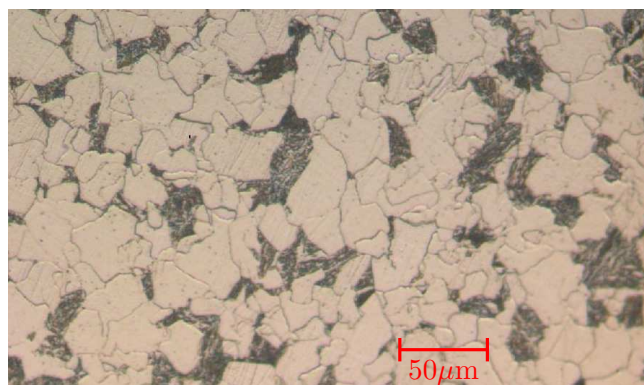


Figure 1: Micrograph of X65 carbon steel.

### 2.2. Sample preparation and experimental procedure

X65 carbon samples of 12mm diameter (surface area 1.131cm<sup>2</sup>) were sectioned to 5mm thickness with the non-working surface soldered and masked in non-conductive epoxy. The test surface was wet abraded using silicon carbide (SiC) papers of 120,

Table 2: Test matrix

Item	Description	Value
Metal specification	X65 carbon steel	
	Surface area Test sample	$2 \times 1.121\text{cm}^2$ 2 per cell
Electrolyte condition	De-ionised water	1,000ml
	Brine conc	3.5 wt% NaCl
	pH	pH3.8
	Over potential	50mV, 100mV & 150mV
	Temperature	30° C
	Duration	24h

320, 600, 800, 1,200 grit in sequence followed by degreasing in acetone and immediately air dried. The electrolyte was prepared in a glass vessel containing 1,000mL de-ionised water and 35g of sodium chloride (NaCl) to create a 3.5% NaCl solution. The solution was purged with CO<sub>2</sub> for over 6h at 30°C before the start of each experiment. The encased sample was then subjected to potentiostatic tests under conditions depicted in Table 2.

The reference electrode used was Ag/AgCl while the counter electrode was manufactured from platinum. The Ivium multichannel potentiostat was used for the 3-electrode cell corrosion experiments.

### 3. Post-experiment analysis

Collected samples were immediately prepared for analysis or stored in a vacuumed desiccated jar. Scanning electron microscopy (SEM) and X-ray Diffraction (XRD) analyses were conducted on corroded surfaces to reveal information on products formed under experimental conditions. This was followed by detailed white light interferometry analysis. The samples for interferometry analysis were thoroughly cleaned in Clarke’s solution and immediately rinsed in de-ionised water before analysis. The Clarke’s solution comprised of 1000 mL hydrochloric acid (HCl), 50g stannous chloride (SnCl<sub>2</sub>) with 20g antimony trioxide (Sb<sub>2</sub>O<sub>3</sub>) in line with the American Standard of Test and Measurements (ASTM) practice standard G1-03 [22].

#### 3.1. Identification of pits and profiling technique

Addressing pitting corrosion problems would not be feasible without a reliable means of identifying, estimating or measuring the extent of pitting [23, 24]. The size, shape and density of corrosion pits are described in ASTM G46-94, Standard guide for examination and evaluation of pitting corrosion [25]. Researchers are more often interested in pit depth measurement owing to the fact that the deepest pit is likely to perforate before others

[24]. The ASTM standard categorises a maximum pit depths of 25 $\mu\text{m}$  (0.025mm) as "light pitting" while pit depth of about 250 $\mu\text{m}$  (0.25 mm) is regarded as "moderate pitting" [24]. Inspectors sometimes consider metal penetration to evaluate the extent of pitting corrosion in either of 2 ways outlined below [26, 27]:

- Height of deepest valley created or preferably, averaging the heights of 10 deepest valleys.
- Pitting factor (Pf) defined as the ratio of deepest valley depth to average metal penetration (determined by weight loss)[28].

Weight loss contribution has often been attributed to general corrosion while ignoring the pitting component. Pitting factor cannot be determined by electrochemical means alone. Electrochemistry / weight loss is needed to measure the general corrosion; Pit details are obtained using profilometry technique. For accuracy, this work took cognizance of weight loss due to pitting, which forms part of overall weight loss. Accuracy of the calculation is high enough for the study of pitting factor as values obtained for 50mV, 100mV and 150mV are reasonably consistent in the repeated test featured in Tables 3 and 4. Pit identification in this work was based on averaging the 10 deepest pits after detailed, repeated systematic scanning of the entire corroded surface as well as reporting the maximum pit depth, in alignment with the ASTM standard.

#### 3.1.1. Profiling technique for pit analysis

Circular samples of 12mm diameter were utilised in this work to maximise the in-built automated capability of the profilometer to perform optimised circular scans without the operator’s interference once a reference coordinate was established. For pitting investigations, it is important to capture the entire surface of a corroded sample to ensure that no pit is missed during the scanning process. A 10mm scan diameter was set for profilometry analysis leaving out only a 1mm edge that was covered in resin during the test. The measurement was programmed to commence from the centre of the sample and scanned outwards in an anti-clockwise direction covering small, discrete areas that extends over the entire area of the sample in 172 measurements. The scanned bits were stitched with 25% overlap setting.

The profilometer implemented enables terms removal, data analysis and multiple region analysis, amongst other tools suitable for analysing corrosion damage on steel samples. The multiple region analysis provides statistics and location of pits, size, volume, diameter, skewness and other data suitable for validating identified pits. The stitching capability of the profilometer enables scanning of a large area (within optimal fringe caption) by adding a series of small datasets in the scan area of suitable dimension. The required data range is determined by selecting suitable thresholds for pit depth and pit pixels. Tools such as  $R_{sk}$ ,  $R_p$  and  $R_v$  measurements amongst others enable further screening of generated data which can be logged and ranked in accordance with the provisions of ASTM standard for corrosion pit evaluation [25]. Analysis conducted on the profilometer were as well guided by the provisions contained in the Measurement Good Practice Guide No. 108 provided by the National Physical Laboratory [29] and other ISO literature. Tests and measurements were repeated at least thrice, to validate data which were germane in arriving at findings presented in this work.

## 4. Results

### 4.1. Effect of applied potential on pitting

The current density transient response of samples subjected to 50mV, 100mV and 150mV potentiostatic (Figure 2) was observed to fluctuate at the start of the experiment until equilibrating after about 7h. For passive steel, Pagitsas [30] suggested that high and low current measured during potentiostatic polarisation respectively reflect the non-protective and protective states of a metal where drop in current would normally imply significant transition of a metal from active to passive state. This however does not apply to carbon steel in this instance, as it remains an actively corroding material throughout the duration of the experiment. At the end of each experiment, distinct pits were visible on each steel surface using SEM. An example of the nature of pits observed under SEM for conditions of 150mV after 24h is provided in Figures 3 and 4.

SEM images of polarised samples revealed that pitting was most abundant at 150mV polarisation. This is sensible given there is a greater driving force to propagate localised attack agreeing with other observations in literature[31]. Measured current den-

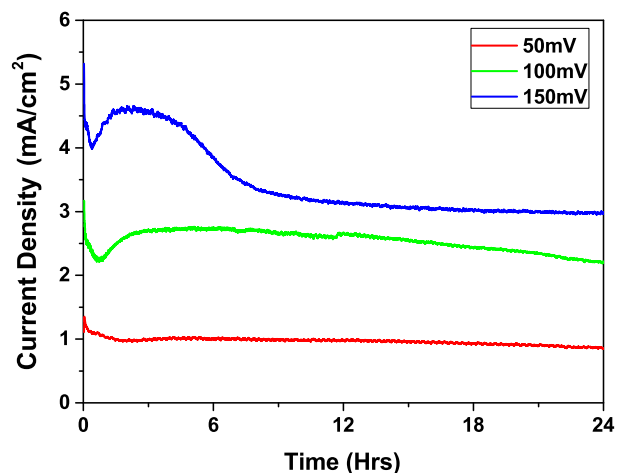


Figure 2: Current transient plot of 50mV, 100mV and 150mV potentiostatic on X65 Carbon steel over a duration of 24h in a 3.5 wt.% NaCl solution saturated with  $CO_2$  at  $30^\circ C$  at pH3.8.

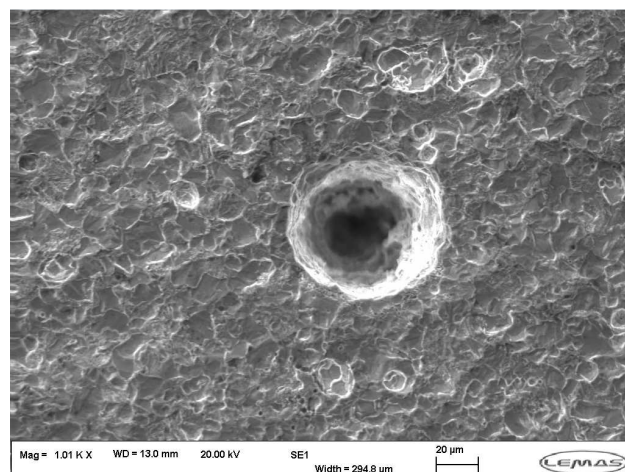


Figure 3: SEM image of pit formed through carbide films on X65 carbon steel under 150mV potentiostatics in 3.5% NaCl solution, pH of 3.8,  $30^\circ C$  for 24h after cleaning with Clarke's solution.

sity in this work could therefore be attributed to general and pitting corrosion. XRD analysis of the surfaces of steel samples subjected to 50mV, 100mV and 150mV potentiostatic revealed presence of iron carbide ( $Fe_3C$  (Figure 5)) which had revealed itself due to the preferential dissolution of the ferrite phase within the steel microstructure. The quantity of  $Fe_3C$  becomes more abundant with increase in the applied potential.

Pits were observed to grow beneath the seemingly fragile and porous  $Fe_3C$  network as shown in Figure 3. This affirms that the  $Fe_3C$  formed was not protective. From the SEM and XRD analysis con-

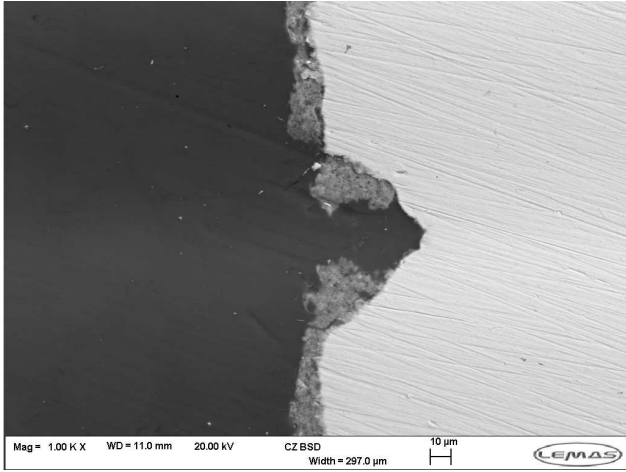


Figure 4: cross section of pit formed through carbide films on X65 carbon steel under 150mV potentiostatics in 3.5% NaCl solution, pH of 3.8, 30°C for 24h.

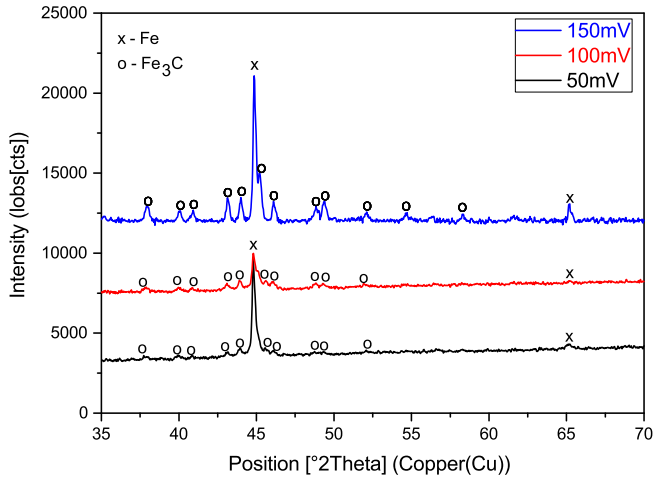


Figure 5: XRD pattern showing Fe<sub>3</sub>C deposit on X65 carbon steel after 50mV, 100mV and 150mV potentiostatic in 3.5% NaCl solution, pH of 3.8, 30°C for 24h

ducted, iron carbonate (FeCO<sub>3</sub>) was not present in the corrosion film as expected under the experimental conditions (i.e. the low pH and low temperature make the FeCO<sub>3</sub> precipitation unfavourable). The environment favoured formation of Fe<sub>3</sub>C films as revealed in the XRD pattern.

#### 4.1.1. Analysis of pitting trend

Profilometry analysis was conducted to determine and quantify the extent of pitting on the polarised X65 carbon steel samples. Pit ranking was done based on pit depth obtained from the multiple region analysis tool of the profilometry software. The morphology of deepest pits recorded under 50mV,

100mV and 150mV polarisation of X65 carbon steel at 30°C, pH3.8 for 24h were 25μm, 55μm and 120μm respectively as shown in Figure 6. The result revealed that pit depth increased with applied anodic potential similar to the pitting trend reported for passive steel polarisation by Tian et al. [32].

The skewness value recorded for generated pits were near zero which indicates a symmetrical pit profile. The interferometry analysis was conducted twice for each set of corroded samples after potentiostatic experiment to ascertain repeatability. Pit depth statistics recorded in Fe<sub>3</sub>C growth conditions under 50mV, 100mV and 150mV potentiostatic is shown in Figure 7. It shows that pit depth increased with increase in applied potential and is able to progress beneath formed product or Fe<sub>3</sub>C as seen in Figure 8.

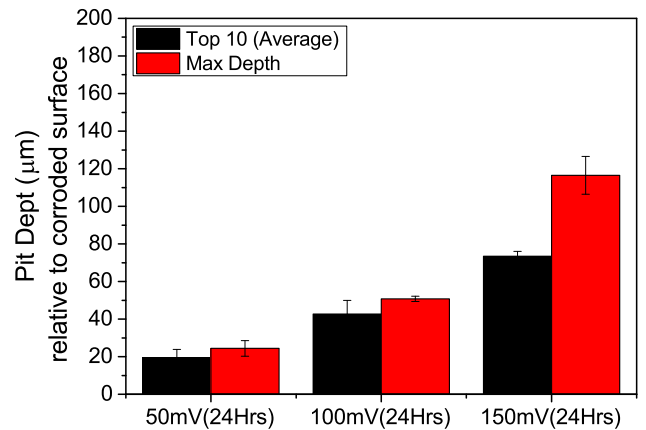
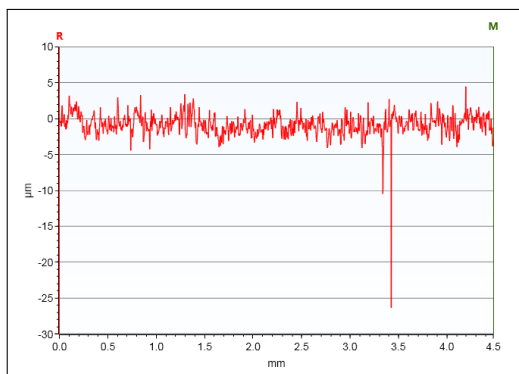


Figure 7: Pit depth chart depicting top-10 average and maximum depth recorded for samples subjected to 50mV, 100mV and 150mV potentiostatic polarisation at 30°C, pH3.8, 3.5wt% NaCl, CO<sub>2</sub> saturated for 24h.

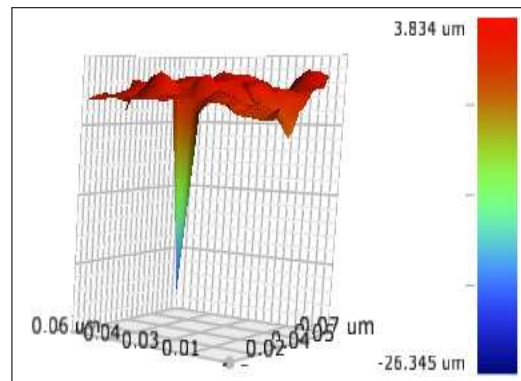
(Note: Max depth (red bars) indicates deepest valley; average of top ten pits (black bars) is termed top-10 average; error bars are based on standard deviation of two set of tests).

#### 4.2. Application of Faraday's law of electrolysis to potentiostatic test result

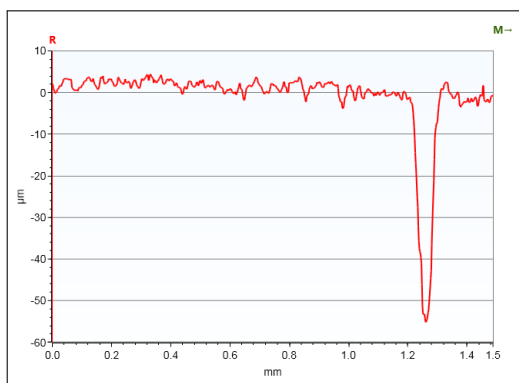
The Butler-Volmer equation provides expression that relates current density to applied potential [33, 34]. Since anodic overpotential of 50mV and beyond were utilised in this work, the anodic exponential term predominates [35, 33, 36] which implies that measured current was solely a measure of applied anodic potential [35] that caused metallic dissolution.



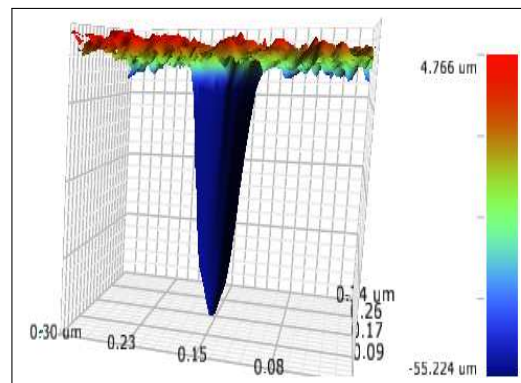
(a) **25 μm** pit (2D) for **50mV** potentiostatic



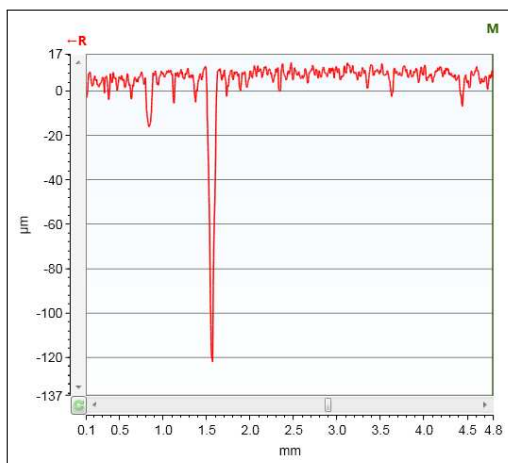
**25 μm** pit (3D) for **50mV** potentiostatic



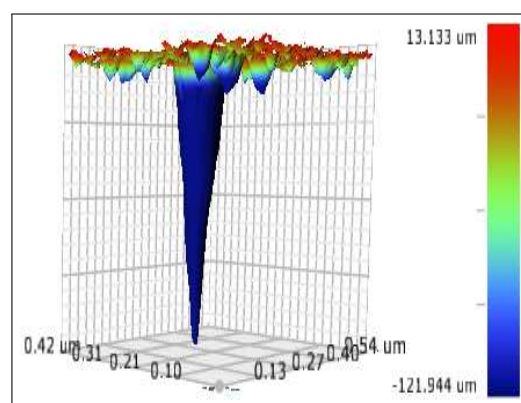
(b) **55 μm** pit (2D) for **100mV** potentiostatic



**55 μm** pit (3D) for **100mV** potentiostatic



(c) **120 μm** pit (2D) for **150mV** potentiostatic



**120 μm** pit (3D) for **150mV** potentiostatic

Figure 6: White light profilometry images showing maximum pit depth recorded on X65 carbon steel after 24h exposure in CO<sub>2</sub> saturated, 3.5% NaCl solution, pH3.8, 30°C under (a) 50mV, (b) 100mV and (c) 150mV polarisation.

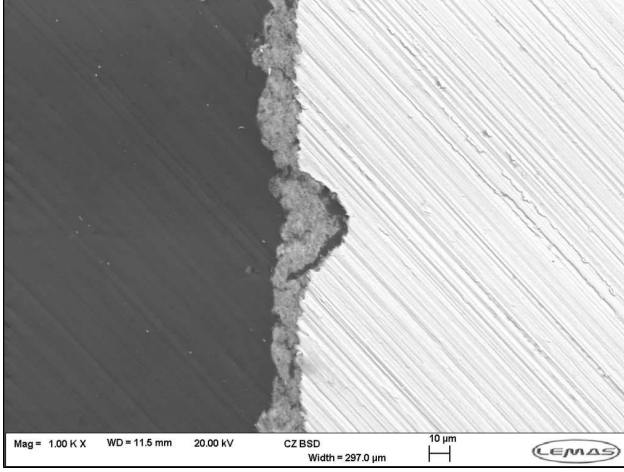
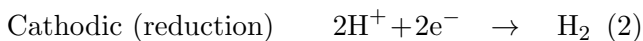


Figure 8: Cross-section morphology of pit formed after 150mV at 3.5% NaCl, 30°C, pH3.8, 24h.

The interferometry software was used to calculate discrete pit volumes. Screened pits in the threshold of  $25\mu\text{m}$  and beyond were considered as true pits in line with ASTM standard for evaluating corrosion test specimens [25]. Pit volume, otherwise termed void volume is the volume of cavity or space created by pit.

Current density measured under potentiostatic conditions accounts for general and pitting corrosion. Void volume derived was then resolved to a mass component based on the density of the steel. Total charge equivalence was obtained by integrating the current transient measurement while Faraday's law was applied to relate charge to associated mass loss. Mass equivalence of void volume was deducted from the overall mass obtained from Faraday's relationship to obtain a mass due to general corrosion.

Potential applied during potentiostatic polarisation perturbs equilibrium thereby forcing electron flow from the anodically polarised electrode which resorts to accelerated corrosion. Anodic polarisation causes oxidation of the electrode (loss of electrons) in accordance with Equation 1 while corresponding cathodic reactions may be complex, but mainly influenced by reactions featured in equations 2 - 4 .



Progressive charge from the electrochemical reaction was calculated from the corrosion density response recorded during 24h potentiostatic experiment by integrating the the product of measured current (I) with time (t) as presented in Equation 5. Electrochemical measurements were taken at intervals of 10 seconds covering 24h test duration.

$$Q = \int_0^{24\text{h}} I dt = \int_0^{24\text{h}} i A dt \quad (5)$$

Where Q is the total charge recorded after 24h potentiostatic test measured at intervals of 10 s, 'i' is current density ( $\text{A}/\text{m}^2$ ) and 'A' is test surface area ( $\text{m}^2$ ). Faraday law was applied to the electrochemical reaction to express relationship between mass and current as given in Equation 6.

$$Q = It = zFn \quad (6)$$

Where Q (Coulombs) is charge involved in the electrochemical process, I is current (Ampere), t is time (seconds), z is number of electrons in one molecule of Fe, F (Faraday's constant) = 96,485 Coulombs/mole and n is the number of reacting mole = reacting mass ( $m$ )/molar mass ( $M$ ). Equivalent weight ( $E_w$ ) is the mass of reacting species that utilises one Faraday charge. This implies that  $E_w = \text{atomic or molecular weight } (M) / \text{valency}(z)$ . Substituting for n in Equation 6 gives Equation 7 [37].

$$m = \frac{MI t}{zF} = \frac{MQ}{zF} = \frac{(E_w)Q}{F} \quad (7)$$

Volume equivalence or void volume (V) can be obtained by substituting for mass in Equation 7 to derive expression in Equation 8, where  $\rho$  is density of carbon steel.

$$Q = \frac{VF\rho}{E_w} = \frac{VFZ\rho}{M} \quad (8)$$

$Q$ , represents the total charge utilised for the entire corrosion process which comprises of uniform and general corrosion. A similar expression was utilised in the work of Tian et al. [21] who investigated potential effect on stainless steel. The volume component therefore reflects void volume for uniform and pitting corrosion that take place on the steel. With  $25\mu\text{m}$  minimum threshold set for pitting categorisation, pitting volume was deducted from the total volume derived from electrochemical results.

Total charge involved during the potentiostatic tests was calculated by integrating parameters in Equation 5. A total charge of approximately 200 Coulomb, 500 Coulomb and 700 Coulomb was involved under 50mV, 100mV and 150mV potentiostatic respectively as depicted in Figure 9.

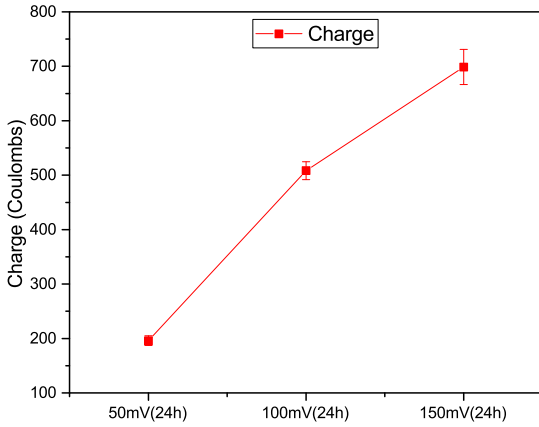


Figure 9: Plot depicting magnitude of charge expended for repeated test of 50mV, 100mV and 150mV potentiostatic at  $30^\circ\text{C}$ , pH3.8, 3.5%wt NaCl for 24h.

Figure 10 shows that no significant pitting was recorded under 50mV. Low pitting but high general corrosion was recorded for 100mV potentiostatic. Pitting and general corrosion were both significant under 150mV potentiostatic. This implies that increase in potentiostatic range increases general corrosion as well as pitting but to different extents.

#### 4.3. Derivation of pitting factor

An acceptable approach to relate pitting extent with general corrosion is by considering pitting factor ( $Pf$ ) as provided in ASTM G46-94 [25]. Pitting Factor is defined as the ratio of deepest valley depth to average metal penetration [28].

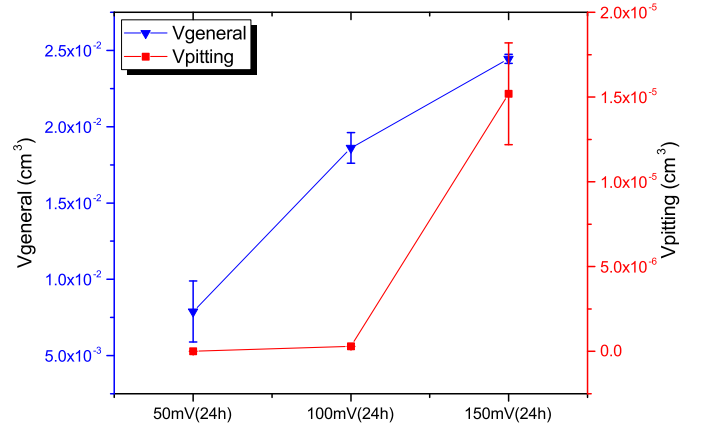


Figure 10: Plot of void volume depicting trend for general and pitting corrosion after 50mV, 100mV and 150mV potentiostatic at  $30^\circ\text{C}$ , pH3.8, 3.5%wt NaCl for 24h.

Pitting factor of unit magnitude indicates general corrosion. Pitting factor basically increases as pitting extent increase. Since general corrosion takes place on the entire test sample surface, the volume of mass corroded ( $Vol_{\text{general}}$ ) is expressed as indicated in Equation 9.

$$Vol_{\text{general}} = \pi r^2 D \quad (9)$$

Where  $r$  is the radius of test sample (ie 0.6cm).  $D$  is therefore calculated for 50mV, 100mV and 150mV potentiostatic tests as tabulated in Tables 3 and 4.

Analysis of the pitting factors contained in Table 3 features  $Pf$  of 1.41, 1.34 and 1.55 for 50mV, 100mV and 150mV potentiostatic polarisation. A repeated test recorded  $Pf$  of 1.21, 1.17 and 1.32 for 50mV, 100mV and 150mV as depicted in Table 4. This indicates that the extent of general corrosion thickness loss compared to pitting depth are quite similar. Interestingly, recorded pitting factor for all polarisation cases fell within values reported on the 7th day test of Pessu et al.[38] who compared pitting and general corrosion under  $30^\circ\text{C}$ ,  $50^\circ\text{C}$ , and  $80^\circ\text{C}$  by naturally developing pits at OCP. Pessu et al. used the same material, temperature ( $30^\circ\text{C}$ ),  $\text{CO}_2$  partial pressure as this work but with a higher pH and a slightly higher NaCl concentration, which could lead to formation of amorphous  $\text{FeCO}_3$ . Such amorphous films do not tend to evolve into dense protective films at low temperature ( $30^\circ\text{C}$ ). Low temperature

retards precipitation [39] which renders amorphous layer porous thereby allowing interaction of the surface with the bulk solution. Experimental conditions employed in this work are however reasonably close to the 30°C investigations made by Pessu et al [38]. This suggests that potentiostatic polarisation gives accelerated corrosion of both general and pitting corrosion instances in reasonable proportion. This implies that potentiostatic polarisation has the potential to be employed for accelerated corrosion processes.

Table 3: Parameters for determining pitting factor (Test 1)

Description	50mV	100mV	150mV
$Vol_{general}(cm^3)$	$6.89 \times 10^{-3}$	$1.81 \times 10^{-2}$	$2.45 \times 10^{-2}$
D (cm) (Equation 9)	$6.09 \times 10^{-3}$	$1.6 \times 10^{-2}$	$2.17 \times 10^{-2}$
$Pit_{max}(cm)$ from interferometry	$2.5 \times 10^{-3}$ (25 $\mu m$ )	$5.5 \times 10^{-3}$ (55 $\mu m$ )	$1.2 \times 10^{-3}$ (120 $\mu m$ )
P (cm) (D + $Pit_{max}$ )	$8.59 \times 10^{-3}$	$2.15 \times 10^{-2}$	$3.37 \times 10^{-2}$
Pf = P/D	1.41	1.34	1.55

Table 4: Parameters for determining pitting factor (Test 2)

Description	50mV	100mV	150mV
$Vol_{general}(cm^3)$	$7.54 \times 10^{-3}$	$1.93 \times 10^{-2}$	$2.69 \times 10^{-2}$
D (cm) (Equation 9)	$6.67 \times 10^{-3}$	$1.71 \times 10^{-2}$	$2.38 \times 10^{-2}$
$Pit_{max}(cm)$ from interferometry	$2.5 \times 10^{-3}$ (25 $\mu m$ )	$5.5 \times 10^{-3}$ (55 $\mu m$ )	$1.2 \times 10^{-3}$ (120 $\mu m$ )
P (cm) (D + $Pit_{max}$ )	$9.16 \times 10^{-3}$	$2.26 \times 10^{-2}$	$3.58 \times 10^{-2}$
Pf = P/D	1.21	1.17	1.32

## 5. Pit growth under active condition

To evaluate the ability of pits formed from the potentiostatic technique to continue to propagate, a series of experiments were performed. The samples polarised at 150mV for 24h were transferred into an unbuffered test solution at 80°C and left for 24 and 48h. Pitting data gathered from extensive profilometry of the steel surface indicated that the pits continues to grow linearly in depth after immersion in the 80°C test solution. These results hold promise in that the technique can potentially be used to help in the understanding of pit propagation within laboratory tests repeatedly and in a reasonable time-frame.

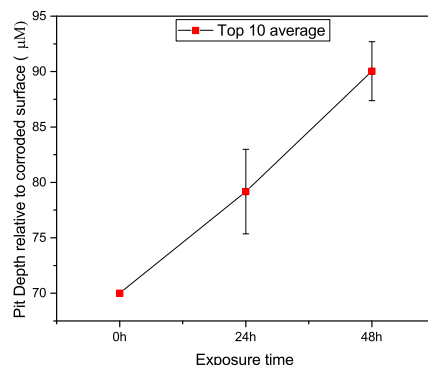


Figure 11: Plot depicting trend of pit from initial depth of 70 $\mu m$  exposed to saturated CO<sub>2</sub> unbuffered solution at 80°C up to 48h.

Figure 11 depicts the growth of pit exposed to unbuffered, saturated CO<sub>2</sub> solution at 80°C. Pit with initial depth of 70 $\mu m$  increased to about 78 $\mu m$  after 24h exposure with further incrementation to 90 $\mu m$  after 48h of exposure. This suggests that general and pitting corrosion progress linearly under the 2-day exposure.

## 6. Conclusions

An investigation into the merits of potentiostatic polarisation for inducing a reproducible pitted surface for pit propagation studies has been performed. The following conclusions can be reached from this work:

- The application of anodic potential was shown to accelerate both general and pitting corrosion, but to different extents (depending upon applied potential) in relation to their contribution towards total material loss from the steel surface.
- Potentiostatic polarisation between 50 and 150mV at pH 3.8 and 30°C in a CO<sub>2</sub> environment was shown to generate reproducible pits, which were stress free.
- Average pit depth increased linearly with increase in applied potential in the range of 50 - 150mV, with 150mV producing the more repeatable and deepest pits averaging 70 $\mu m$ .
- The pitting factors associated with polarised samples agreed with those obtained in literature in similar CO<sub>2</sub> environments, demonstrating that

polarisation of the sample produces the correct balance between the relative thickness losses associated with both general and pitting corrosion on the steel surface for continued pit propagation studies.

- e. Transfer of the polarised samples into test solutions at 80°C for 48h showed that the developed pits continued to propagate, indicating the potential of this technique to assist in performing pit propagation studies in reasonable time-frames.

## Acknowledgment

Thanks to the Petroleum Technology Development Fund (PTDF) for financial support to the first author.

## References

- [1] Y. Hua, R. Barker, A. Neville, Effect of temperature on the critical water content for general and localised corrosion of x65 carbon steel in the transport of supercritical co<sub>2</sub>, *International Journal of Greenhouse Gas Control* 31 (2014) 48–60.
- [2] G. Zhang, Y. Cheng, Localized corrosion of carbon steel in a co<sub>2</sub>-saturated oilfield formation water, *Electrochimica Acta* 56 (3) (2011) 1676–1685.
- [3] S. Nešić, Key issues related to modelling of internal corrosion of oil and gas pipelines—a review, *Corrosion Science* 49 (12) (2007) 4308–4338.
- [4] S. Papavinasam, A. Doiron, R. W. Revie, Model to predict internal pitting corrosion of oil and gas pipelines, *Corrosion* 66 (3) (2010) 035006–035006.
- [5] X. Jiang, S. Nešić, B. Kinsella, B. Brown, D. Young, Electrochemical investigation of the role of cl-on localized carbon dioxide corrosion behavior of mild steel, *Corrosion* 69 (1) (2012) 15–24.
- [6] G. S. Frankel, N. Sridhar, Understanding localized corrosion, *Materials Today* 11 (10) (2008) 38–44.
- [7] A. Turnbull, D. Coleman, A. Griffiths, Assessment of test methods for evaluating effectiveness of corrosion inhibitors in retarding propagation of localised corrosion, *British Corrosion Journal* 36 (3) (2001) 210–214.
- [8] P. Zhang, Z. Liu, Physical-mechanical and electrochemical corrosion behaviors of additively manufactured cr-ni-based stainless steel formed by laser cladding, *Materials & Design* 100 (2016) 254–262.
- [9] J. Zhang, D.-H. Yang, X.-B. Ou, Microstructures and properties of aluminum film and its effect on corrosion resistance of az31b substrate, *Transactions of Nonferrous Metals Society of China* 18 (2008) s312–s317.
- [10] B. Fang, R. Eadie, W. Chen, M. Elboujdaini, Passivation/immersion method to grow pits in pipeline steel and a study of pit nucleation and growth resulting from the method, *Corrosion Engineering, Science and Technology* 44 (1) (2009) 32–42.
- [11] R. Newman, The dissolution and passivation kinetics of stainless alloys containing molybdenum. dissolution kinetics in artificial pits, *Corrosion Science* 25 (5) (1985) 341–350.
- [12] S. Zhou, A. Turnbull, Development of pre-pitting procedure for turbine disc steel, *British Corrosion Journal* 35 (2) (2000) 120–124.
- [13] A. Turnbull, D. Coleman, A. Griffiths, P. Francis, L. Orkney, Effectiveness of corrosion inhibitors in retarding the rate of propagation of localized corrosion, *Corrosion* 59 (3) (2003) 250–257.
- [14] J. W. Palmer, J. Marsh, R. C. Newman, et al., Evaluation of inhibitor performance for protection against localized corrosion, in: *CORROSION 2002, NACE International*, 2002.
- [15] J. Han, B. Brown, S. Nešić, Investigation of the galvanic mechanism for localized carbon dioxide corrosion propagation using the artificial pit technique, *Corrosion* 66 (9) (2010) 095003–095003.
- [16] J. Amri, E. Gulbrandsen, R. Nogueira, Pit growth and stifling on carbon steel in co<sub>2</sub>-containing media in the presence of hac, *Electrochimica Acta* 54 (28) (2009) 7338–7344.
- [17] R. Miresmaeili, A. Abdollah-Zadeh, et al., The mutual effects of hydrogen and microstructure on hardness and impact energy of sma welds in x65 steel, *Materials Science and Engineering: A* 679 (2017) 87–94.
- [18] I. M. Robertson, P. Sofronis, A. Nagao, M. Martin, S. Wang, D. Gross, K. Nygren, Hydrogen embrittlement understood, *Metallurgical and Materials Transactions B* 46 (3) (2015) 1085–1103.
- [19] M. Dadfarnia, A. Nagao, S. Wang, M. L. Martin, B. P. Somerday, P. Sofronis, Recent advances on hydrogen embrittlement of structural materials, *International Journal of Fracture* 196 (1-2) (2015) 223–243.
- [20] R. P. Gangloff, Probabilistic fracture mechanics simulation of stress corrosion cracking using accelerated laboratory testing and multi-scale modeling, *Corrosion* 72 (7) (2016) 862–880.
- [21] W. Tian, S. Li, N. Du, S. Chen, Q. Wu, Effects of applied potential on stable pitting of 304 stainless steel, *Corrosion Science* 93 (2015) 242–255.
- [22] ASTM, G1 - Standard practice for preparing, cleaning, and evaluating corrosion test specimens, *ASTM International*, 2011.
- [23] E. Morikawa, O. Kizilkaya, R. S. Perkins, Infrared characterization of localized corrosion products, *Infrared Physics & Technology* 51 (5) (2008) 407–409.
- [24] D. W. Hoepfner, pitting corrosion: Morphology and characterization, *framework* 25 (1985) 26.
- [25] ASTM, G46-94, Standard Guide for Examination and Evaluation of Pitting Corrosion, *ASTM International*, West Conshohocken, PA, 2005.
- [26] M. G. Fontana, *Corrosion engineering*, Tata McGraw-Hill Education, 2005.
- [27] G. H. Koch, M. P. Brongers, N. G. Thompson, Y. P. Virmani, J. H. Payer, *Corrosion cost and preventive strategies in the united states*, Tech. rep. (2002).
- [28] R. Pierre, *Handbook of corrosion engineering* (1999).
- [29] N. P. Library, *Guide for the measurement of smooth surface topography using coherence scanning interferometry*, A National measurement good practice guide Number

108.

- [30] M. Pagitsas, A. Diamantopoulou, D. Sazou, A point defect model for the general and pitting corrosion on iron oxide electrolyte interface deduced from current oscillations, *Chaos, Solitons & Fractals* 17 (2) (2003) 263–275.
- [31] L. R. Hilbert, Monitoring corrosion rates and localised corrosion in low conductivity water, *Corrosion Science* 48 (12) (2006) 3907–3923.
- [32] W. Tian, S. Li, N. Du, S. Chen, Q. Wu, Effects of applied potential on stable pitting of 304 stainless steel, *Corrosion Science* 93 (2015) 242–255.
- [33] E. McCafferty, Validation of corrosion rates measured by the tafel extrapolation method, *Corrosion Science* 47 (12) (2005) 3202 – 3215, a Century of Tafels Equation: A Commemorative Issue of Corrosion Science. doi:<https://doi.org/10.1016/j.corsci.2005.05.046>.  
URL <http://www.sciencedirect.com/science/article/pii/S0010938X05002374>
- [34] K. Uddin, L. Somerville, A. Barai, M. Lain, T. Ashwin, P. Jennings, J. Marco, The impact of high-frequency-high-current perturbations on film formation at the negative electrode-electrolyte interface, *Electrochimica Acta* 233 (2017) 1–12.
- [35] H. J. Flitt, D. P. Schweinsberg, Evaluation of corrosion rate from polarisation curves not exhibiting a tafel region, *Corrosion Science* 47 (12) (2005) 3034 – 3052, a Century of Tafels Equation: A Commemorative Issue of Corrosion Science. doi:<https://doi.org/10.1016/j.corsci.2005.06.014>.  
URL <http://www.sciencedirect.com/science/article/pii/S0010938X05002143>
- [36] W. S. Tait, An introduction to electrochemical corrosion testing for practicing engineers and scientists, PairODocs Publications, 1994.
- [37] Z. Ahmad, Chapter 3 - corrosion kinetics, in: Z. Ahmad (Ed.), *Principles of Corrosion Engineering and Corrosion Control*, Butterworth-Heinemann, Oxford, 2006, pp. 57 – 119. doi:<https://doi.org/10.1016/B978-075065924-6/50004-0>.
- [38] F. Pessu, R. Barker, A. Neville, Understanding pitting corrosion behavior of x65 carbon steel in co<sub>2</sub>-saturated environments: The temperature effect, *Corrosion* 72 (1) (2015) 78–94.
- [39] M. Kermani, A. Morshed, Carbon dioxide corrosion in oil and gas productiona compendium, *Corrosion* 59 (8) (2003) 659–683.